Proceeding Paper

Experiments on Damage and Failure Behavior of Biaxially Loaded Specimens under Non-Proportional Load Paths †

Moritz Zistl * , **Steffen Gerke and Michael Brünig**

Institut für Mechanik und Statik, Universität der Bundeswehr München, Werner-Heisenberg-Weg 39, D-85577 Neubiberg, Germany

* Correspondence: moritz.zistl@unibw.de; Tel.: +49-89-6004-2095

† Presented at the 19th International Conference on Experimental Mechanics, Kraków, Poland, 17–21 July 2022.

Abstract: This paper discusses new experiments with the X0-specimen taken from steel sheets and numerical simulations to investigate the influence of proportional and non-proportional loading on damage and failure processes in the moderate stress state regime. The numerical simulations were based on a phenomenological, thermodynamically consistent anisotropic continuum damage model considering the effect of stress triaxiality and the Lode parameter on damage behavior. The proportional and non-proportional loading histories were compared and analyzed. During the experiments, digital image correlation (DIC) was used to assess strain fields on the surface of the specimens, while scanning electron microscopy allowed for an analysis of fracture surfaces (SEM). Numerical simulations reveal stress distributions and the evolution of stress states during the load path. The findings show the effectiveness of the experimental program for highly ductile metals, the accuracy of the presented continuum model as well as the influence of loading history on damage and failure behavior in steel sheets.

Keywords: ductile metals; biaxial experiments; damage; digital image correlation; non-proportional loading

1. Introduction

Ductile sheet metals are of high relevance as raw material in many forming processes and environmental and economic requirements have led to increased research activities during the last decades to develop high quality alloys. To minimize the localization of irreversible strains and to prevent damage or failure of structural elements under various loading conditions and loading histories, material strengths must be increased. Consequently, the modeling of constitutive behavior and numerical simulation of deformation, damage processes and failure are essential parts of production processes. It has been observed in several experiments and engineering applications that the formation of large inelastic and often localized deformations caused by dislocations on microscopic slip planes are accompanied by nucleation, growth and the coalescence of micro-defects. These mechanisms on the micro-scale depend on stress states and on loading histories. In order to create reliable continuum models, systematic studies of the are stress-state-dependent and loading-path-dependent phenomena are necessary. In this aspect, results of experiments with different specimen geometries have been described in the literature. To explore the stress-state dependent damage and fracture processes, for instance, uniaxial tests with unnotched and differently notched specimens and corresponding numerical simulations have been carried out [1–5]. In addition, tests with various cruciform specimens were carried out to examine more stress states and facilitate various loading histories because these uniaxially loaded specimens only cover a limited range of stress [6–13]. The findings show that the loading history has a significant influence on the formation of damage and fracture processes, which requires further investigation. In this context, new experiments with the biaxial the X0-specimen [14] and corresponding numerical simulations

undergoing different non-proportional loading histories have been performed [15,16]. The present paper extends those investigations with X0-specimens taken from sheets of the steel alloy X5CrNi18-10 undergoing non-proportional loading and fracture under moderate stress states. A continuum damage model is discussed which considers the macroscopic effect of different damage mechanisms through stress-state-dependent functions. In the experiments, the formation of strain fields in critical locations of the specimens was measured using the digital image correlation (DIC) method. Scanning electron microscopy (SEM) of fractured surfaces was used to explore fracture mechanisms. Numerical simulations indicate stress distributions that contribute to various damage processes and failure mechanisms on the micro-level.

2. Continuum Damage Model

The continuum damage model proposed by Brünig [17] was used to analyze damage and fracture behavior in ductile metals. The kinematic approach, which introduces elastic, plastic, and damage strain rate tensors, is based on the introduction of damaged and fictitious undamaged configurations. Plastic behavior is defined in the undamaged configurations, without the influence of damage degradation and is characterized by the yield criterion

$$f^{\text{pl}} = \sqrt{\bar{J}_2} - c = 0, \tag{1}$$

with the second invariant $\bar{J}_2 = \frac{1}{2}\text{dev}\overline{\mathbf{T}}\cdot\text{dev}\overline{\mathbf{T}}$, of the effective Kirchhoff stress tensor $\overline{\mathbf{T}}$ and the equivalent yield stress c. The evolution of plastic deformations is predicted by an isochoric plastic strain rate

$$\dot{\overline{\mathbf{H}}}^{\text{pl}} = \dot{\gamma}\overline{\mathbf{N}} \tag{2}$$

In the undamaged configurations, where $\overline{\mathbf{N}} = \left(1/\sqrt{2\bar{J}_2}\right)\text{dev}\overline{\mathbf{T}}$, a normalization of the effective deviatoric stress tensor and the equivalent plastic strain measure is represented by γ. Furthermore, the damage criterion

$$f^{\text{da}} = \alpha I_1 + \beta\sqrt{J_2} - \sigma = 0 \tag{3}$$

represents models onset and the continuation of damage and is defined in the damaged configurations. It is written in terms of the first stress invariant $I_1 = \text{tr}\mathbf{T}$ and the second deviatoric invariant $J_2 = \frac{1}{2}\text{dev}\mathbf{T}\cdot\text{dev}\mathbf{T}$ of the Kirchhoff stress tensor $\mathbf{T}$. The material toughness against the propagation of micro-defects is denoted by σ. The parameters α and β in Equation (3) are damage mode functions considering the different form of damage mechanisms acting on the micro-level and are dependent on the stress triaxiality

$$\eta = \frac{I_1}{3\sqrt{3J_2}} \tag{4}$$

as well as on the Lode parameter

$$\omega = \frac{2T_2 - T_1 - T_3}{T_1 - T_3} \text{ with } T_1 \geq T_2 \geq T_3 \tag{5}$$

expressed in terms of the principal values T_1, T_2 and T_3 of the Kirchhoff stress tensor. In addition, the damage strain rate tensor

$$\dot{\mathbf{H}}^{\text{da}} = \dot{\mu}\left(\bar{\alpha}\frac{1}{\sqrt{3}}\mathbf{1} + \bar{\beta}\mathbf{N}\right) \tag{6}$$

predicts damage induced by the evolution of inelastic strains, where μ represents a measure for equivalent damage strain and $\mathbf{N} = (1/\sqrt{2J_2})\text{dev}\tilde{\mathbf{T}}$ is the normalized deviatoric stress tensor. Here, parameters $\bar{\alpha}$ and $\bar{\beta}$ are stress-state-dependent kinematic functions denoting

the volumetric and isochoric damage-induced strain rates corresponding to the different damage and failure mechanisms on the micro-level.

3. Experiments and Corresponding Numerical Simulations

The experiments were carried out using the biaxial test setup depicted in Figure 1a. It has four electromechanically driven cylinders with a load capacity of ± 20 kN. The specimens were clamped in the heads of the cylinders. The digital image correlation (DIC) method was used to quantify three-dimensional displacement fields in selected regions of the specimens during the tests. The stereo setting contained six 6.0 Mpx cameras (LIMESS, Krefeld, Germany) with 75 mm lenses and corresponding lighting system (Fomex, Seoul, Korea, FL-B50 LED-panel lights with 1600 lx on both sides) as shown in Figure 1b. For the correlation process, a subset size of 33 px with a grid spacing of 11 px and the software Istra4D by Dantec Dynamics GmbH (Skovlunde, Denmark) were used.
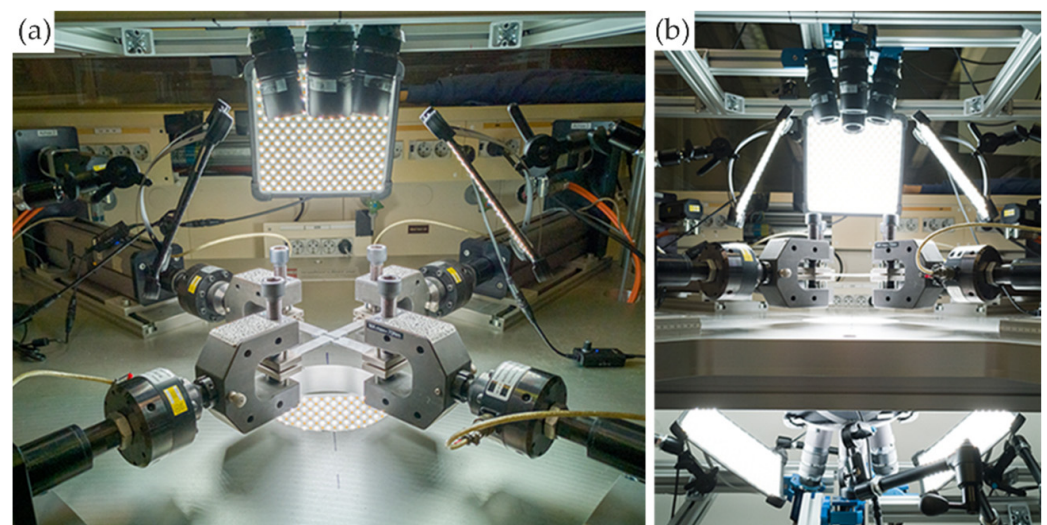
Figure 1. (**a**) Biaxial setup, (**b**) System for digital image correlation with lighting and cameras.

The steel alloy X5CrNi18-10 (EN 10088-3) is the subject of the investigation, and specimens were cut from sheets with a 4 mm thickness. The biaxial X0-specimen in Figure 2a–c includes four notched sections that are tilted at $45°$ and a central hole. Displacement fields were examined in this area by DIC. The specimen had a thickness of 2 mm at its thinnest points and measured 240 mm along each axis. The depth of the notches was 1 mm. The test routine considered biaxial loading of the specimen by F_1 and F_2 and the movement of the red dots (Figure 2d), $u_{1.1}$ and $u_{1.2}$ in 1-direction and $u_{2.1}$ and $u_{2.2}$ in 2-direction served as displacement measure $\Delta u_{ref.1} = u_{1.1} - u_{1.2}$ and $\Delta u_{ref.2} = u_{2.1} - u_{2.2}$. The loading paths of this series can be seen in Figure 2e. In the first case, the specimen was proportionally loaded by $F_1 : F_2 = 1 : -0.5$ and a maximum load of $F_1 = -2F_2 = 14.0$ kN. For the non-proportional case, the specimen was firstly loaded by F_1 up to $F_1 = 9.5$ kN, then it was kept constant and subsequently in axis 2, the loading F_2 decreased to $F_2 = -5.0$ kN. The point of axis switch takes place at 20% of the fracture displacement of the corresponding proportional experiment $F_1 : F_2 = 1 : 0$. The influence of the first non-proportional section on the overall experiment is thus small compared to an axis switch shortly before fracture. The last step of the load path is proportional loading up to fracture.
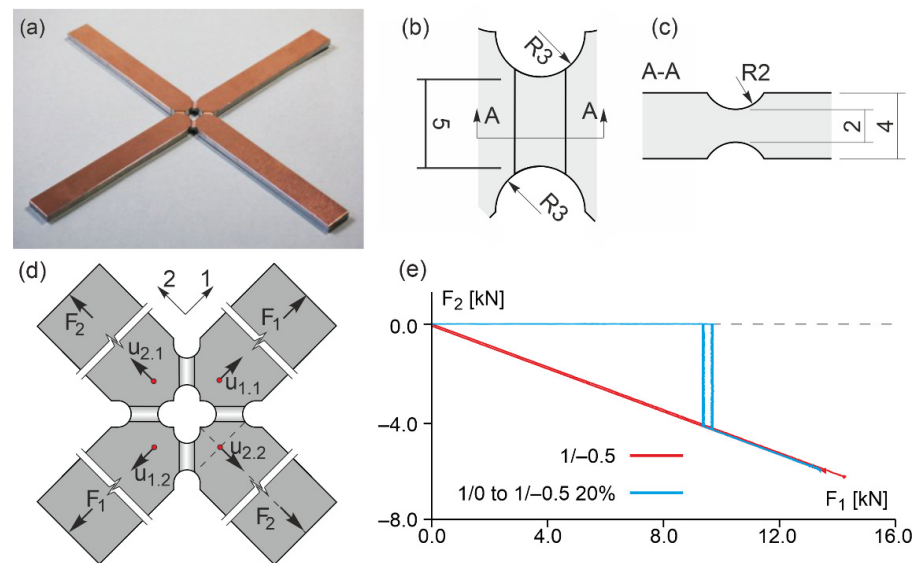
Figure 2. X0-specimen (dimensions in mm): (**a**) photo, (**b**) notch detail, (**c**) notch cross section, (**d**) definition of forces and displacements, (**e**) investigated loading path.

3.1. Numerical Aspects

The numerical simulations were carried out utilizing ANSYS, which was enhanced by a user-defined material subroutine based on the constitutive equations of the proposed continuum damage model. Time integration of the constitutive rate in Equations (2) and (6) was performed by an inelastic predictor–elastic corrector scheme [18]. For the spatial discretization of the specimen, one symmetry quarter of the geometry was meshed with eight-node-elements of type solid185. Within the notched area, a mesh size of 0.1 mm was set.

### 3.2. Results of Experiments and Numerical Simulations

Good agreement between the results of the experiments and the corresponding numerical simulations can be seen in the force-displacement plots for the proportional case (Figure 3a) and the non-proportional case (Figure 3b).
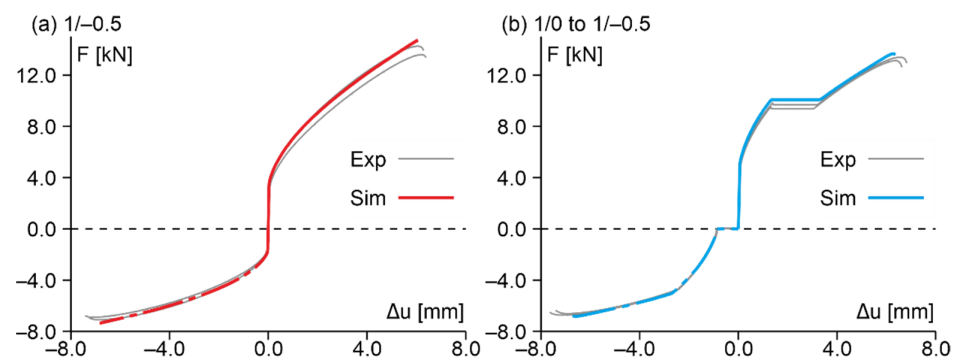
Figure 3. Force-displacement plots of experiment and simulation (axis 1 solid lines, axis 2 dash-dotted lines): (**a**) $1/-0.5$, (**b**) $1/0$ to $1/-0.5$.

Additionally, Figure 4 compares the first principal strain fields in the notched area of the X0-specimen. Just before fracture of the proportional loaded specimen (P $1/-0.5$ end), large strains of up to 122% were measured in the experiment (Exp). They distribute in a tilted, elliptical band. This distribution was qualitatively predicted by the simulation (Sim), with only slightly smaller maxima (103%). On the other hand, in the non-proportional loading path, a slightly more localized band with an orientation from top left to bottom right

was measured in the experiment after the first load step (NP 1/0 to 1/−0.5 switch) with a maxima of 25%. Just before fracture in the non-proportional path (NP 1/0 to 1/−0.5 end), a rotation of the localized band and its extension to the edges takes place, whereby the qualitative distribution resembles the proportional load path. The strains reach values of up to 128% in the center. In the numerical simulation (Sim) this distribution was also predicted but with slightly smaller maxima. The strain fields in Figure 4 demonstrate that even for a minor non-proportional part within a load path, the loading history affects the deformation and localization behavior of the examined steel.
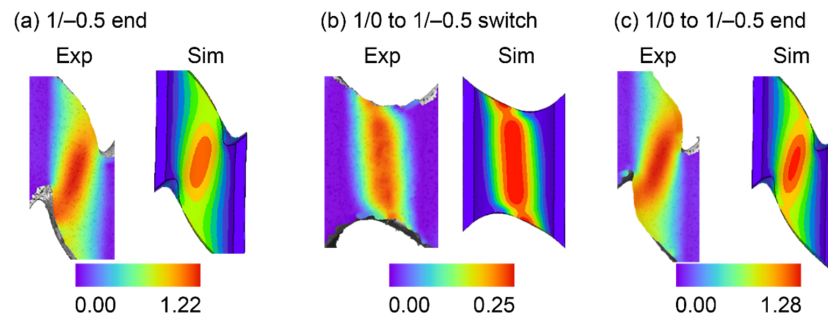
Figure 4. First principal strain fields of the notch surface for the DIC measurements (respectively left) and the numerical simulations (respectively right) for load cases 1/−0.5 (**a**) and 1/0 to 1/−0.5 (**b**,**c**).

A result of the numerical simulations is the stress state and its predicted distribution over the cross section of a notch is displayed through the stress triaxiality in Figure 5. Here, only proportional loading results in a minimum stress triaxiality of $\eta = 0.15$ in the center. At the boundaries (Figure 5a), an increase to $\eta = 0.4$ can be seen. The Lode parameter is $\omega = -0.6$ in the center and at the boundaries of the notch $\omega = -1$ (Figure 5d). In the non-proportional loaded simulation, more moderate values of $\eta = 0.25$ are predicted in the central area of the cross section and $\eta = 0.4$ at its border at the time of axis switch (Figure 5b). Correspondingly, values of the Lode parameter are around $\omega = -0.6$ (Figure 5e). Shortly before fracture occurs, the stress triaxiality increases to around $\eta = 0.25$ in the central part and $\eta = 0.4$ at the border (Figure 5c). The values of the predicted Lode parameter are between $-1.0 \leq \omega \leq -0.6$ (Figure 5f). Thus, the stress state just before fracture is only marginally influenced by a non-proportional loading path.
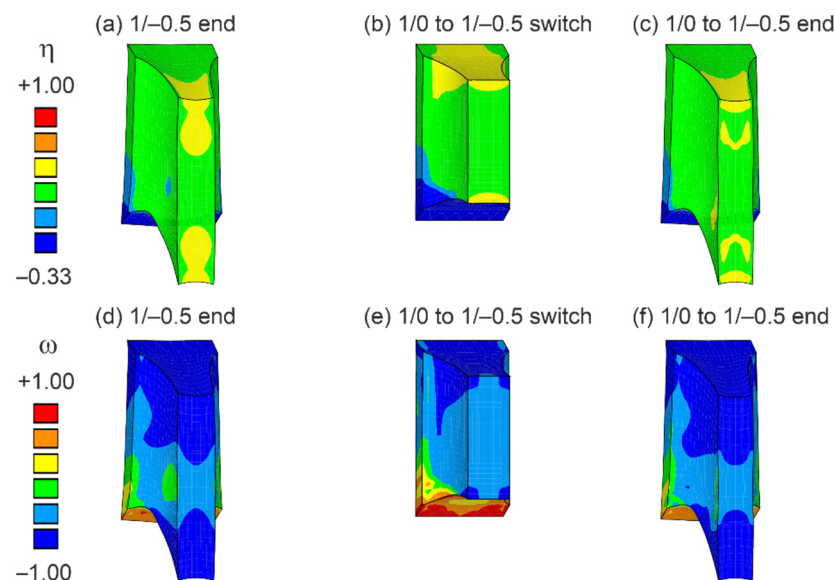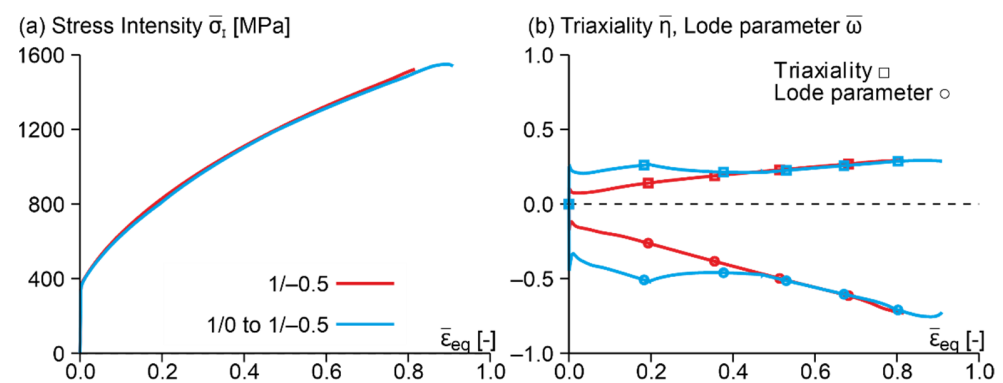

Figure 5. Distribution of stress triaxiality η and Lode parameter ω over cross section of notch for load cases 1/−0.5 (**a**,**d**) and 1/0 to 1/−0.5 (**b**,**c**,**e**,**f**).

The change in the stress state during the different load paths is plotted in Figure 6. In Figure 6a, the mean value of the stress intensity $\overline{\sigma_I}$ over the cross section of a notch is calculated, with the stress intensity being defined as

$$\sigma_I = \max(|T_1 - T_2|, |T_2 - T_3|, |T_3 - T_1|) \tag{7}$$

in terms of the principal components of the Kirchhoff stress tensor. This mean value is plotted as a function of the mean value of the von Mises equivalent strain $\overline{\varepsilon}_{eq}$. Similarly, in Figure 6b the evolution of mean value of stress triaxiality $\overline{\eta}$ and mean value of Lode parameter $\overline{\omega}$ are displayed as functions of $\overline{\varepsilon}_{eq}$. Overall, the mean values in Figure 6b differ only in the first load step. After axis switch ($\overline{\varepsilon}_{eq} = 0.2$), the mean value of stress triaxiality of the non-proportionally loaded specimen aligns very fast with the only proportionally loaded one. This again indicates a rather short influence of the first load step on the overall damage and failure behavior.


Figure 6. Predicted evolution of mean stress intensity $\overline{\sigma_I}$ as function of mean equivalent strain $\overline{\varepsilon}_{eq}$ (**a**) as well as mean stress triaxiality $\overline{\eta}$ and Lode parameter $\overline{\omega}$ over mean equivalent strain $\overline{\varepsilon}_{eq}$ (**b**) over the cross section of a notch.

The spatial distribution of plastic equivalent strain γ and damage equivalent strain μ is displayed in Figure 7. In Figure 7a,b, the plastic equivalent strain forms similarly in a slightly tilted, elliptical shape, but with a 10% increased maximum strain of 1.41 at the center of the surface ($1/0$ to $1/-0.5$ end). This tendency is also visible in the tilted elliptical distribution of μ. Here, maxima are predicted on the surface, but an increase of 25% between Figures 7b and 7d to 0.20 is noted. This significant increase in equivalent damage strain compared to equivalent plastic strain might be a result of the first load step with increased stress triaxiality (Figure 5) and indicates a load path dependency of damage behavior.

Furthermore, in Figure 8 the images of the fractured notch surfaces taken by scanning electron microscopy are displayed. For the proportional load path, clear traces of shear processes are visible due to the smooth surfaces and plumes at the pore craters (Figure 8a). This behavior is presumably caused by the numerically predicted low stress triaxiality. For the first loading step in the non-proportional load path, a moderate stress triaxiality was predicted (Figure 5b). This should result in shearing mechanisms superimposed with void growth. The stress triaxiality decreases in the subsequent load steps, but the influence of the initial moderate one remains visible due to the significant increase in voids as shown in Figure 8b. As a result, the loading history has an impact on the failure and damage processes at the micro level.
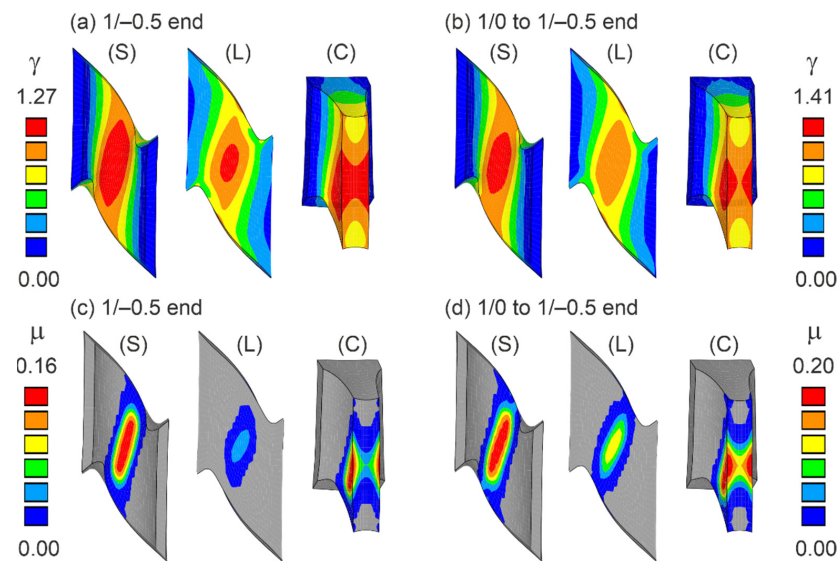
Figure 7. Spatial distribution of equivalent plastic strain γ and equivalent damage strain μ on the surface (S), in the longitudinal section (L) and the cross section (C) of a notch for load cases $1/-0.5$ (**a**,**c**) and $1/0$ to $1/-0.5$ (**b**,**d**).
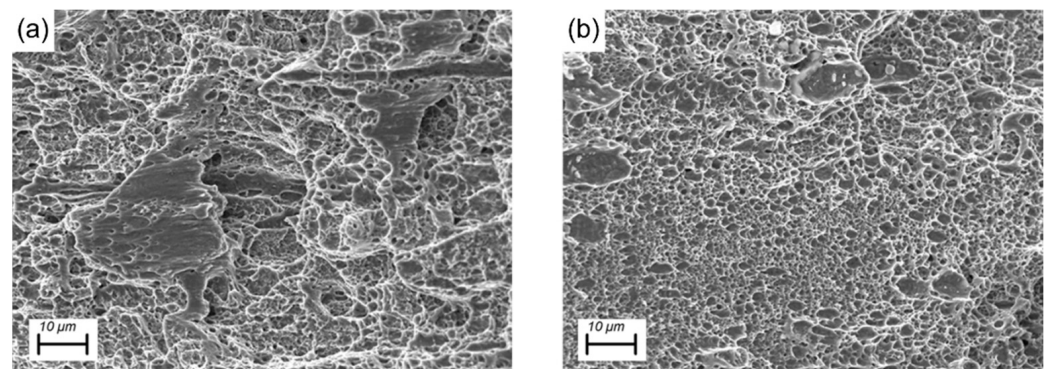
Figure 8. Pictures from scanning electron microscopy of the fracture surfaces for load cases $1/-0.5$ (**a**) and $1/0$ to $1/-0.5$ (**b**).

4. Conclusions

In this paper, a continuum framework to model the damage evolution of ductile materials was briefly discussed. The phenomenological model takes into account various branches in the damage criteria and damage rules corresponding to various stress-state-dependent damage and failure processes on the micro-scale. The rate equations that model the evolution of plastic and damage strains are numerically integrated using the inelastic predictor–elastic corrector approach. New experiments with biaxially loaded X0-specimens extracted from steel sheets were used to validate the continuum damage model, and the results were compared to those obtained from the corresponding numerical simulations. The studies concentrated on biaxial loading conditions and different loading paths with the same final loading ratio, resulting in moderate stress triaxiality. The analysis revealed an influence of even small non-proportional sections in a loading history on the damage and failure behavior in ductile steels compared to proportional ones. The predicted differences in stress states during non-proportional loading lead to different stress-state-dependent damage processes on the micro-level and were visualized by scanning electron microscopy of fractured surfaces. The evolution of damage and fracture mechanisms is already affected by small non-proportional sections in a load path. As a result, the influence of loading history has to be considered in the validation of accurate material models predicting the failure and lifetime of engineering structures and forming processes.

References

1. Bao, Y.; Wierzbicki, T. On fracture locus in the equivalent strain and stress triaxiality space. *Int. J. Mech. Sci.* **2004**, *46*, 81–98. [CrossRef]
2. Bonora, N.; Gentile, D.; Pirondi, A.; Newaz, G. Ductile damage evolution under triaxial state of stress: theory and experiments. *Int. J. Plast.* **2005**, *21*, 981–1007. [CrossRef]
3. Driemeier, L.; Brünig, M.; Micheli, G.; Alves, M. Experiments on stress-triaxiality dependence of material behavior of aluminum alloys. *Mech. Mater.* **2010**, *42*, 207–217. [CrossRef]
4. Gao, X.; Zhang, G.; Roe, C. A Study on the effect of the stress state on ductile fracture. *Int. J. Damage Mech.* **2010**, *19*, 75–94. [CrossRef]
5. Roth, C.C.; Mohr, D. Ductile fracture experiments with locally proportional loading histories. *Int. J. Plast.* **2016**, *79*, 328–354. [CrossRef]
6. Chow, C.L.; Lu, T.J. An analytical and experimental study of mixed-mode ductile fracture under nonproportional loading. *Int. J. Damage Mech.* **1992**, *1*, 191–236. [CrossRef]
7. Green, D.E.; Neale, K.W.; MacEwen, S.R.; Makinde, A.; Perrin, R. Experimental investigation of the biaxial behaviour of an aluminum sheet. *Int. J. Plast.* **2004**, *20*, 1677–1706. [CrossRef]
8. Kulawinski, D.; Nagel, K.; Henkel, S.; Hübner, P.; Fischer, H.; Kuna, M.; Biermann, H. Characterization of stress–strain behavior of a cast TRIP steel under different biaxial planar load ratios. *Eng. Fract. Mech.* **2011**, *78*, 1684–1695. [CrossRef]
9. Kuwabara, T. Advances in experiments on metal sheets and tubes in support of constitutive modeling and forming simulations. *Int. J. Plast.* **2007**, *23*, 385–419. [CrossRef]
10. Brünig, M.; Zistl, M.; Gerke, S. Numerical analysis of experiments on damage and fracture behavior of differently preloaded aluminum alloy specimens. *Metals* **2021**, *11*, 381. [CrossRef]
11. Dunand, M.; Mohr, D. Optimized butterfly specimen for the fracture testing of sheet materials under combined normal and shear loading. *Eng. Fract. Mech.* **2011**, *78*, 2919–2934. [CrossRef]
12. Lian, J.; Liu, W.; Gastañares, X.; Juan, R.; Mendiguren, J. Plasticity evolution of an aluminum- magnesium alloy under abrupt strain path changes. *Int. J. Mater. Form.* **2022**, *15*, 40. [CrossRef]
13. Kong, X.; Helfen, L.; Hurst, M.; Hänschke, D.; Missoum-Benziane, D.; Besson, J.; Baumbach, T.; Morgeneyer, T.F. 3D in situ study of damage during a 'shear to tension' load path change in an aluminium alloy. *Acta Mater.* **2022**, *231*, 117842. [CrossRef]
14. Gerke, S.; Adulyasak, P.; Brünig, M. New biaxially loaded specimens for the analysis of damage and fracture in sheet metals. *Int. J. Solids Struct.* **2017**, *110*, 209–218. [CrossRef]
15. Gerke, S.; Zistl, M.; Bhardwaj, A.; Brünig, M. Experiments with the X0-specimen on the effect of non-proportional loading paths on damage and fracture mechanisms in aluminum alloys. *Int. J. Solids Struct.* **2019**, *163*, 157–169. [CrossRef]
16. Gerke, S.; Zistl, M.; Brünig, M. Experiments and numerical simulation of damage and fracture of the X0-specimen under non-proportional loading paths. *Eng. Fract. Mech.* **2020**, *224*, 106795. [CrossRef]
17. Brünig, M. An anisotropic ductile damage model based on irreversible thermodynamics. *Int. J. Plast.* **2003**, *19*, 1679–1713. [CrossRef]
18. Brünig, M. Numerical analysis of anisotropic ductile continuum damage. *Comput. Methods Appl. Mech. Eng.* **2003**, *192*, 2949–2976. [CrossRef]